Electronic Density of States of Noncrystalline Si and Ge: I. Spherically Symmetric Interference Function Approach

N. C. Halder and R. L. Wourms

Department of Physics, University of South Florida, Tampa, Florida 33620

(Z. Naturforsch. **30 a**, 55–63 [1975]; received September 24, 1974)

The electronic density of states have been calculated for amorphous and liquid phases of Si and Ge, using pseudopotential perturbation theory. These calculations are carried out on the basis of experimental radial distribution functions for the appropriate phases, and second order in electron energy. The density of states generated by this method compare favorably with those obtained by other computational methods.

I. Introduction

One of the practical attempts to calculate the density of states of amorphous semiconductors was made by Herman and Van Dyke [1] under the assumption that the amorphous material would be nearly 30% less dense than the corresponding crystalline phase. As a result, their calculation led to a larger atomic spacing to allow for the lower atomic density and to semimetal conduction. The expanded crystal model seems to have been abandoned, and it is now commonly believed that the structure of amorphous Si and Ge is a random tetrahedral network. The central atom and its four nearest neighbors form a distorted tetrahedron. The tetrahedral bonds are randomly oriented with respect to each other. The orientations of these bonds range from the extreme eclipsed to the staggered configuration [2]. To satisfy these conditions of the atomic structure, the first two peaks of the radial distribution function (RDF) are sufficient. This conclusion is in accord with the experimental results (see, for example, Herman et al. [3] and Mott and Davis [4]). Computer simulated RDF with as many as 64 atoms in this configuration have produced results in qualitative agreement with experiment.

McGill and Klima [5] have calculated the density of states assuming that the atoms of amorphous Si and Ge are clustered in groups of 8 in tetrahedral bonding in the eclipsed or staggered configuration. Cohen et al. [6] have suggested that in amorphous semiconductors the density of states has an overlap; the conduction and valence bands have tails of localized states sufficiently extensive to overlap near the center of the mobility gap. An alternative model has been proposed by Mott and Davis [4] which has a fairly narrow band of localized states, less than 0.1 eV, near the center of the gap. It is believed that the previously observed states were due to unsatisfied bonds (i. e., all atoms are not bound to four nearest neighbors in a tetrahedral bonding), interstitial, and so on.

There is another type of approach in which an amorphous solid is considered to be a collection of microcrystallites with some amount of short range order and very small particle size, about 10 to 30 A. Recently, Tsay et al. [7] used this model to determine optical properties of amorphous Si and Ge, and found results in good agreement with experiments.

The purpose of this investigation is two-fold. First, is to examine the pseudopotential perturbation theory which has been so extensively used in calculating the electronic properties of simple metals [8]. Second, is to obtain the density of states in amorphous Si and Ge from the experimental information we have about their respective RDF. One of the reasons for undertaking the present research work is determine whether a perturbation method can give the electron density of states, effective mass and electron energy comparable to the results obtained by other methods and also by experiments. In this work, the RDF will be used in the second order perturbation theory to calculate the electron energy. We shall also compute the results for liquid Si and Ge and compare them with those of corresponding amorphous states. The format of our paper will be as follows. In Section II, we shall outline the theoretical approach. In Section III, we shall present our results and discussions. Finally, we shall summarize the important points in the light of the present investigation.

II. Method of Calculation

The pseudopotential perturbation theory has been successfully applied to study the electronic structure

and band properties of many metals, but it was not so successful in the case of crystalline semiconductors [8] with diamond structure, particularly in Si. However, the many-OPW treatment of Si using the same pseudopotential has met with reasonable success [9] with regard to its band structure calculation, and interpretation of the band gaps between the occupied and unoccupied states. These results have led one to suspect that for Si while many-OPW treatment leads to a semiconducting behavior, a straightforward application of the perturbation theory gives rise to a metallic conduction. A critical discussion about this point has been made in a review article by Heine and Weaire [10]. Cohen and Bergestresser [11] have done a detailed calculation of the pseudopotential matrix elements of Si and Ge and studied the band properties of these two elements. Quite recently, Joannopoulos and Cohen [12] have extended these pseudopotential results to investigate the density of states with the tight binding model proposed earlier by Weaire [13] and Weaire and Thorpe [14] for amorphous semiconductors. On the other hand, Kramer [15] employed the pseudopotentials in the Green's functions theory to obtain the density of states and optical absorptions of amorphous Si and Ge. His results are in reasonable agreement with experiments.

From the above summary, two things are quite clear for Si and Ge: first is that the applicability of the pseudopotentials in the tight binding as well as in the Green's function theory is reasonably well established and second is that the validity of the pseudopotential perturbation theory is still not clear. We shall start our subsequent arguments with this premise.

The main reason for considering previously the perturbation theory inappropriate in crystalline Si and Ge was that in the low momentum transfer region the pseudopotential matrix elements $w(q)$ are rather large. Evidently, the success of the perturbation theory will surely depend upon the selection of the potential and the number of higher order terms those are to be retained in the perturbation series. In the present work, we shall use the second order perturbation theory instead, but point out that we are interested only in the amorphous state and not in the crystalline solid. Our arguments applicable to the amorphous state will be analogous to those of the liquid state. When Si and Ge undergo from crystalline to amorphous phase transformation, the discrete Bragg peaks of the crystalline state will disappear at the expense of the appearance of a continuous, oscillatory interference function $I(q)$ whose first, second and third maxima will be found approximately about the same positions as the first three reciprocal lattice vectors of the crystalline state. In Table 1, we show the $w(q)$ and $I(q)$ data for the first three reciprocal lattice vectors. These $I(q)$ values are taken from experimental measurements of amorphous Si and Ge (see Refs. [16] and [17]). For the second order perturbation theory to be appropriate it will be sufficient if it turns out that the ratio $I(q)w^2(q)/E_F \ll 1$.

Table I. The Data at the Reciprocal Lattice Vectors Corresponding to First Three of the Crystalline State.

$q/2\,k_F$	$w(q)$ (Ry)	$I(q)$	$I(q)w^2(q)$	$I(q)w^2(q)/E_F$
For Si: $E_F=0.92$ Ry, $k_F=0.941$ au				
0.553	−0.211	0.30	1.336×10^{-2}	1/69
0.903	0.040	1.40	2.240×10^{-3}	1/411
1.058	0.081	1.75	1.148×10^{-2}	1/80
For Ge: $E_F=0.85$ Ry, $k_F=0.911$ au				
0.551	−0.232	0.25	1.345×10^{-2}	1/63
0.901	−0.011	0.95	1.150×10^{-4}	1/7671
1.056	0.060	1.65	5.940×10^{-3}	1/143

We show all these values as well in Table 1. In the small q limit, but below the first reciprocal lattice vector, also the applicability of the perturbation theory can be easily tested. This is illustrated in Fig. 1 which shows that the first peak maximum of $I(q)$ falls to the left of the first node of $w(q)$. In this respect, this situation is equivalent to that of a pure monovalent metal, like for example Na.

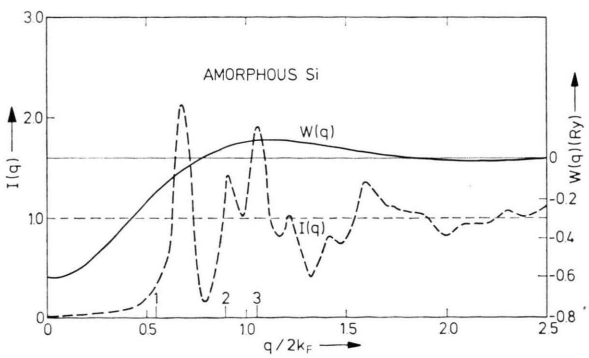

Fig. 1. The plots of $I(q)$ and $w(q)$ for amorphous Si. The numbers 1, 2 and 3 represent the positions of the first three reciprocal lattice vectors respectively. Similar curves can be obtained for amorphous Ge, which are not shown here.

Similar result can be obtained for amorphous Ge, which is not shown here for the sake of compactness. It is well known that for metals, with the increase of valence, the first peak maximum of $I(q)$ moves to the right of the first node of $w(q)$. The perturbation theory is found to be less appropriate in metals with valence 4 and higher, where the first maximum of $I(q)$ falls to the right of the first node of $w(q)$.

In the present investigation, we are not interested in the band gaps of the usual Bragg type, i. e., scattering due to periodicity of the crystalline state. Only the "bond" gaps of the chemical type resulting from the covalent bonds and their deviations will be pertinent [18–21]. These gaps will also include the interactions of the nearest neighbors. Furthermore, we shall assume that the local pseudopotential and experimental RDF are adequate to describe the physical situations in amorphous Si and Ge. Therefore, by utilizing the usual perturbation theory [22, 23] to second order, we obtain the electron energy,

$$E(\boldsymbol{k}) = \frac{\hbar^2 k^2}{2m} + \langle \boldsymbol{k} | W | \boldsymbol{k} \rangle + \sum_{q}{}' \frac{\langle \boldsymbol{k}+\boldsymbol{q} | W | \boldsymbol{k} \rangle \langle \boldsymbol{k} | W | \boldsymbol{k}+\boldsymbol{q} \rangle}{(\hbar^2/2m)(k^2 - |\boldsymbol{k}+\boldsymbol{q}|^2)} . \quad (2.1)$$

The prime over the summation excludes the term with $q = 0$. It is generally argued that a calculation beyond the second order energy is unneccessary and it seldom justifies the computer time required.

In the spirit of "rigid ion model" approximation the matrix elements may be written as [15]

$$\langle \boldsymbol{k}+\boldsymbol{q} | W | \boldsymbol{k} = S(\boldsymbol{q}) \langle \boldsymbol{k}+\boldsymbol{q} | w | \boldsymbol{k} \rangle , \quad (2.2)$$

where

$$\langle \boldsymbol{k}+\boldsymbol{q} | w | \boldsymbol{k} \rangle = \Omega_0^{-1} \int \exp\{i\,\boldsymbol{q}\cdot\boldsymbol{r}\}\, w(\boldsymbol{r})\, \mathrm{d}^3 r , \quad (2.3)$$

$$S(\boldsymbol{q}) = N^{-1} \sum_{j} \exp\{i\,\boldsymbol{q}\cdot\boldsymbol{r}_j\} , \quad (2.4)$$

and N is the number of ions in the volume Ω_0. Here $S(\boldsymbol{q})$ is the usual structure factor depending only on the ion position, and $\langle \boldsymbol{k}+\boldsymbol{q} | w | \boldsymbol{k} \rangle$ is the form factor [24], which depends only on the ion potential. Using this type of form factor, the first order energy $E^{(1)}$ may be expressed as

$$E^{(1)} = \lim_{q\to 0} N^{-1} \sum_{\nu} \exp\{i\,\boldsymbol{q}\cdot\boldsymbol{R}_\nu\}\, w(q) = w(0) \quad (2.5)$$

where $w(0)$ has been normalized to include the self consistent field by dividing it with the Hartree dielectric constant. The second order energy $E^{(2)}$ can be obtained in the same manner,

$$E^{(2)} = \sum_{\boldsymbol{k}'}{}' \frac{I(|\boldsymbol{k}-\boldsymbol{k}'|)\, w^2(|\boldsymbol{k}-\boldsymbol{k}'|)}{(k^2 - k'^2)} , \quad (2.6)$$

where

$$I(q) = N^{-1} \langle \sum_{\nu\mu} \exp\{i\,\boldsymbol{q}\cdot(\boldsymbol{R}_\nu - \boldsymbol{R}_\mu)\} \rangle \quad (2.7)$$

is the interference function.

The interference functions mentioned in the above equations deserve some mention here. In order to see how they come about, and whether these functions are appropriate in the amorphous phase, we go into some detail here. The concept of $I(q)$ was developed from the x-ray diffraction theory [25], but was carried over with little change to electron diffraction in solids. This model does not allow inelastic collisions between electrons and ions in the lattice. The hard sphere model [26] for liquids has been found adequate for most computational needs. However, there is an additional requirement in the case of amorphous solid, since there is some short range order that must be included in the hard sphere model. The experimental $I(q)$ are free of this difficulty and they can be obtained from the experimental RDF,

$$4\pi r^2 \varrho(r) = 4\pi r^2 \varrho_0 + \frac{2r}{\pi} \int_0^\infty q[I(q) - 1] \sin(qr)\, \mathrm{d}q \quad (2.8)$$

which can be easily Fourier transformed. In the above equations $\varrho(r)$ is the radial density and ϱ_0 is the uniform density of atoms in the solid.

The density of states may now be determined for spherical Fermi surfaces,

$$\frac{g(E)}{g_0(E)} = 2k \left(\frac{\delta E}{\delta k}\right)^{-1} = \left[1 + \frac{1}{2k}\left(\frac{\delta E^{(2)}}{\delta k}\right)\right]^{-1} \quad (2.9)$$

where $g_0(E)$ is the free electron density of states. The details of the computational method and related procedures are the same as in our previous works [22, 23].

III. Results and Discussions

A) Data Processing and Reliability Criterion

Three distinct calculations have been made, because the RDF were taken from three sources: the exeprimental [16, 17], the computer simulated [27], and the hard-sphere-model liquid [26]. The experimental

values were chosen for the amorphous phase. The hard sphere model provided a simple set of data which could be used to check the computer programs, and to test the extreme case of amorphous solids with no short range order. The Henderson-Herman [27] computer simulated RDF were used, since these RDF were generated from the distorted tetrahedral model with 64 atoms. These RDF would be tested against the experimental RDF later on in this section. The reliability of the final result will depend on the reliability of the various RDF and the pseudopotential matrix elements used in this work. The experimental RDF often contains some unavoidable errors due to measuring difficulty and truncation of the Fourier integral at some finite limit (here, $r = 10\text{A}$). It is, therefore, quite necessary to check this step before proceeding with any calculations for the density of states. First thing we did was to "refine" the experimental data. This is briefly illustrated as follows:

In order to explain the physics of the refinement procedure the equation for the interference function was rewritten as

$$I(q) = 1 + \int_0^\infty 4\pi r^2 [\varrho(r) - \varrho_0] \frac{\sin(qr)}{(qr)} \, dr . \quad (3.1)$$

Then two new functions were defined by

$$G(r) = 4\pi r [\varrho(r) - \varrho_0] \quad (3.2)$$

and

$$F(q) = q[I(q) - 1] , \quad (3.3)$$

so that

$$G(r) = \frac{2}{\pi} \int_0^\infty F(q) \sin(qr) \, dq \quad (3.4)$$

and

$$F(q) = \int_0^\infty G(r) \sin(qr) \, dr . \quad (3.5)$$

A procedure worked out by Kaplow et al. [28] allows generation of $F(q)$ from $G(r)$ and vice versa. This is based on function $G(r)$ which is clearly defined in the region of small r, say r less than some critical value r_c. Below r_c, the radial density $\varrho(r)$ is zero, which yields

$$G(r) = -4\pi r \varrho_0 . \quad (3.6)$$

We have adjusted all $G(r)$ to that of Eq. (3.6) below r_c. By making a number of Fourier transforms, we could obtain $I(q)$ which were free of uncertainty and errors in the large q region. It should be noted that small r corresponds to large q region.

The input RDF are shown in Figs. 2 through 3. The interference functions $I(q)$ were evaluated from the corresponding experimental RDF. These are also shown in Figs. 4 and 5. It should be remarked that these $I(q)$ have many more oscillations than one would expect from pure liquids (the hard sphere $I(q)$ for these elements are not shown here for lack of space). Presence of so many of these small oscillations is an indication of the occurrence of small local order in the amorphous phase. The

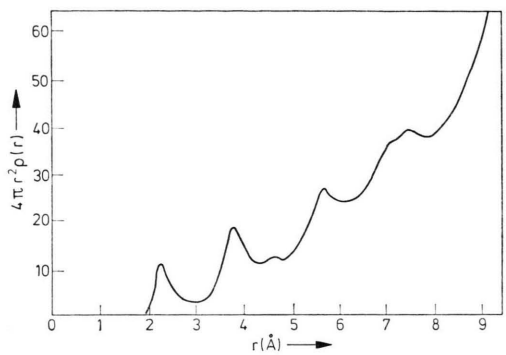

Fig. 2 a. Experimental radial distribution function of amorphous Si. The data were taken from Moss and Graczyk and were 'refined' by successive Fourier transformations.

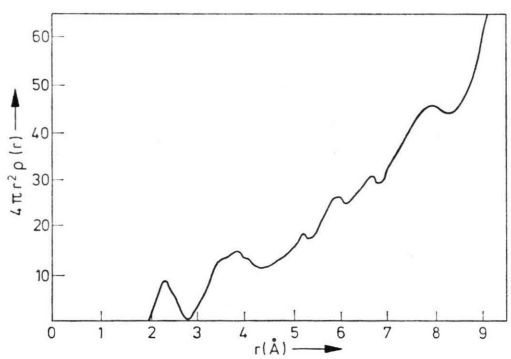

Fig. 2 b. Computer simulated radial distribution function of amorphous Si after Henderson and Herman with $R_0 = 2.35$ A.

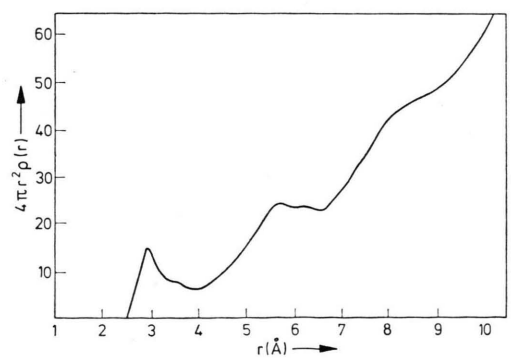

Fig. 2 c. Hard sphere radial distribution function of liquid Si.

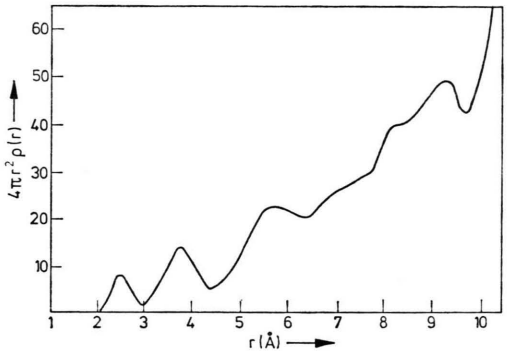

Fig. 3 a. Experimental radial distribution function of amorphous Ge. The experimental data were taken from Richter and Breitling and were 'refined' by successive Fourier transformations.

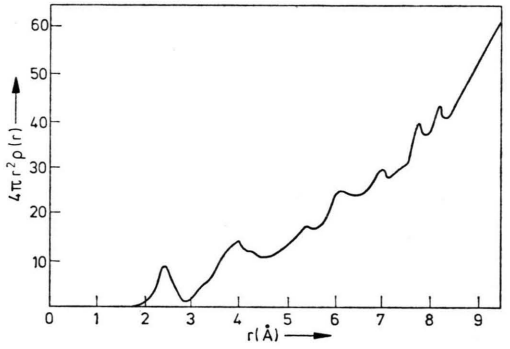

Fig. 3 b. Computer simulated radial distribution function of amorphous Ge after Henderson and Herman with R_0= 2.45 A.

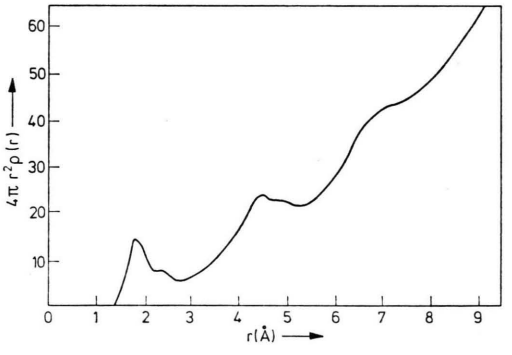

Fig. 3 c. Hard sphere radial distribution function of liquid Ge.

computer simulated $I(q)$ derived from the Henderson-Herman [27] model were quite different in the sense that they had fewer number of oscillations, and the second and third maxima were not well resolved. Moreover, the peak heights were also much reduced compared to the experimental $I(q)$.

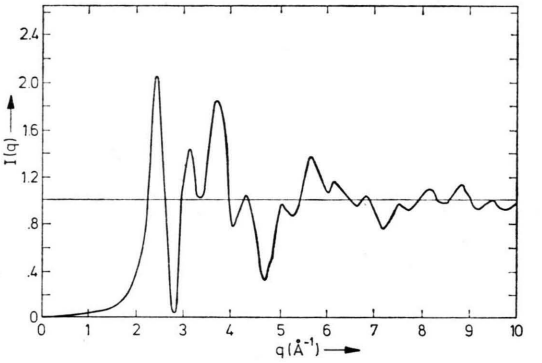

Fig. 4. Interference function of amorphous Si.

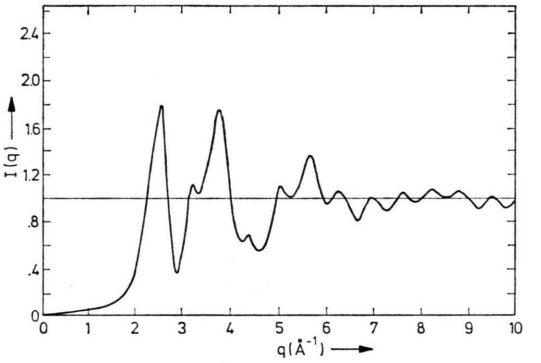

Fig. 5. Interference function of amorphous Ge.

B) Calculated Energy Values

The second order energy values obtained with experimental RDF are shown in Figs. 6 and 7. The zero and first order energy do not depend on k and, therefore, they will not contribute to the density of states. The first order energy is constant at -0.590361 Ryd for Si and at -0.553441 Ryd for

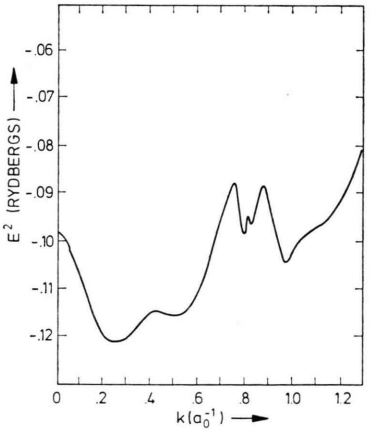

Fig. 6. $E^{(2)}(k)$ for amorphous Si.

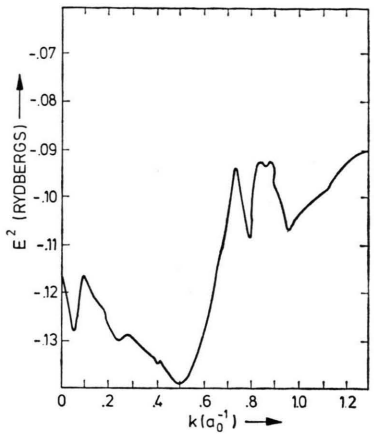

Fig. 7. $E^{(2)}(k)$ for amorphous Ge.

Ge. The second order energy is considerably smaller, but negative and varies with k. It is the derivative of $E^{(2)}(k)$ which will be of our present interest. $E^{(2)}(k)$ for Si is devoid of sharp features. On the other hand, $E^{(2)}(k)$ for Ge has a sharp minimum at $k = 0.05\ a_0^{-1}$ and a sizable peak at $k = 0.9\ a_0^{-1}$. In what follows next, we will see what effects these features have on the density of states.

C) Density of States

The density of states results are plotted in Figs. 8 through 12. Our calculated results in Figs. 8 and 11 lend themselves to direct comparison with the published results, particularly the theoretical plots of Kramer [15] in Fig. 9 and the experimental plots of Pierce and Spicer [19], and Spicer and Donovan [18] in Figs. 10 and 12. Examination of Fig. 8 shows that there is a marked distinction between our results and those (the Green's function) of Kramer [15]. Both the experimental and theoretical values for amorphous Si contain some interesting structures.

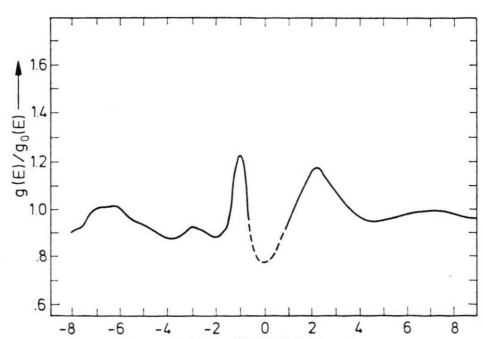

Fig. 8 a. The density of states for amorphous Si obtained from curve 2 a; experimental data [17].

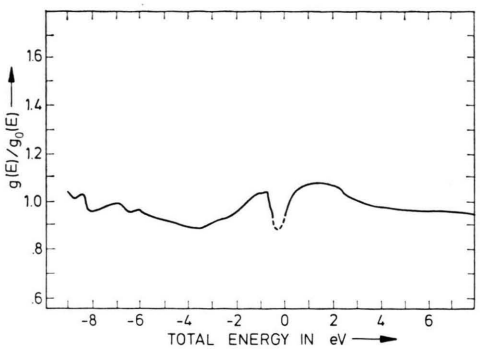

Fig. 8 b. The density of states for amorphous Si obtained from curve 2 b; theoretical values [27].

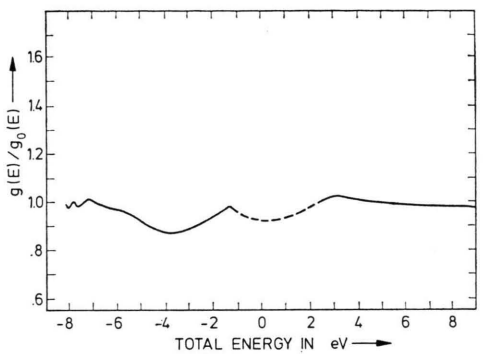

Fig. 8 c. The density of states for liquid Si obtained from curve 2 c; theoretical data.

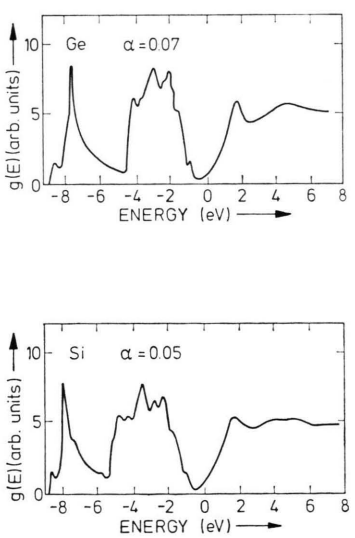

Fig. 9. The theoretical density of states of Kramer for amorphous Si and Ge.

However, liquid Si has a featureless density of states as would be expected from the $E^{(2)}(k)$ plot. All the three results have a minimum near $E = 0$. The existence of a minimum in the density of states near

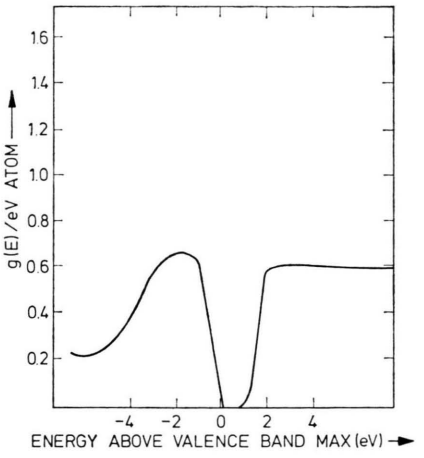

Fig. 10. The experimental density of states of Pierce and Spicer for amorphous Si.

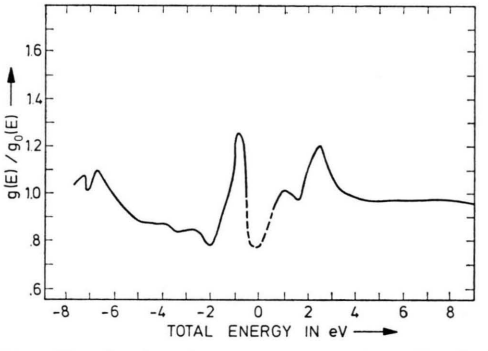

Fig. 11 a. The density of states for amorphous Ge obtained from curve 3 a; experimental data [16].

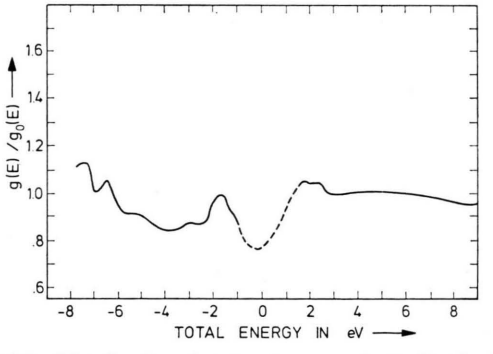

Fig. 11 b. The density of states for amorphous Ge obtained from curve 3 b; theoretical values [27].

$E = 0$ in our results, and that in the experimental results of Pierce and Spicer [19], predicts the possible occurrence of a band gap. In the positive energy region there is a peak near 2 eV in all the three cases. Figure 8(a) shows a small peak near 7 eV compared to the peak at 4.5 eV noted by Kramer [15].

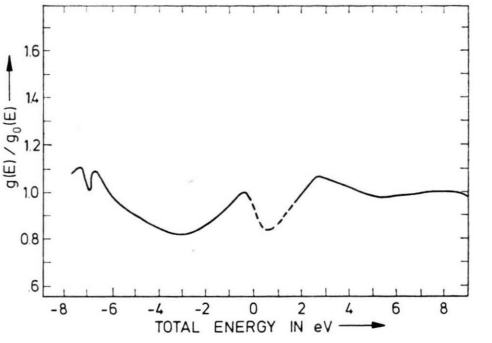

Fig. 11 c. The density of states for liquid Ge obtained from curve 3 c; theoretical data.

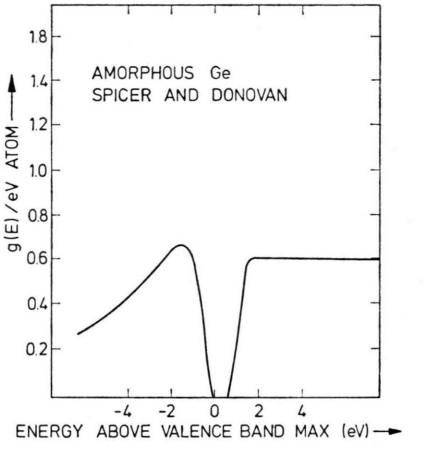

Fig. 12. The experimental density of states of Spicer and Donovan for amorphous Ge.

On the negative energy side, our calculation for amorphous Si shows a peak near -1 eV against the peak near -3 eV observed by Kramer [15]. At more negative values, below -3 eV, our plots do not show any additional structures.

Our results for Ge are ilustrated in Fig. 11 and may be compared with the experimental results of Spicer and Donovan [18] and the theoretical (the Green's function) results of Kramer [15]. The results for liquid Ge are rather striking, because they possess kinks at $E = -7$, 0.5 and 3 eV. The kink observed at $E = -7$ eV is present in all the three Ge samples, but it is not shown in the works of Spicer and Donovan [18] (outside their energy range) or Kramer [15]. On the positive energy side, our plot has somewhat more structure than either of the previous results. The density of states obtained from the Henderson-Herman [27, 29] model are interesting, since they seem to fall between the liquid and the amorphous values. In this case, the minimum is

Tab. II. Results of Effective Mass.

Semi-conductor	Data (RDF) Source	Temp. (°C)	$k_F (a_0^{-1})$	m^*/m
Ge	Hard-sphere liquid model	958	0.9111	1.0617
	Richter-Breitling experiment	23	0.9111	1.2018
	Henderson and Herman Histogram	28	0.9111	1.0127
	Experiment crystal	−269		1.59 (long)
				0.082 (trans)
Si	Hard-sphere liquid model	1400	0.9410	1.0280
	Moss-Graczyk experiment	23	0.9410	1.1250
	Henderson and Herman Histogram	23	0.9410	1.0299
	Experiment crystal	−269		0.98 (long)
				0.19 (trans)

shifted to $E = -1$ eV, the peak in the positive region is shifted to $E = 0.5$ eV and the peak in the negative region is shifted to $E = -1.7$ eV accompanied by some reduction in their respective heights.

D) Effective Mass at Fermi Energy

Electrons in solids, crystals and amorphous semiconductors, may behave as if they have a mass different from the free electron mass. This effective mass is a band structure effect and may be obtained from the above density of states at the Fermi energy [23]. The values of the effective mass are listed in Table 2. It was also our intention to include the effective mass of electrons in the liquid state as determined experimentally, but such an experiment does not appear to have been done at present. In Table 2 "long" and "trans" are the longitudinal and transverse components of the effective mass respectively (see, for example, Kittel [30]). This distinction is necessary when considering the electrons in crystals, since the energy surfaces may be spheroidal, and not spherical as we have assumed in our calculation. Another important factor in the effective mass comparison is the temperature at which the effective mass was calculated. It should be noted that the values of the experimental results, obtained at room temperature, differ from the values obtained for the liquid at the melting point by less than 20%. In general, we would except the effective mass to approach unity as the temperature increases, particularly since Si and Ge both become conductors in the liquid state. The values derived from the Henderson-Herman [27] model seem to be relatively low, but perhaps this difference can be eliminated by modifying their histogram for the simulated RDF, or by increasing the range of r to include distances greater than 8A.

IV. Conclusions

In summary, we find that the perturbation theory to second order along with the experimental RDF give interesting results of the electronic density of states for both amorphous and liquid phases of Si and Ge.

These results are in close agreement with those calculated recently by more sophisticated techniques, such as, the tightbinding and the Green's function theory. While in this work we do not actually find a sharp, well defined gap as has been experimentally seen, we predict the position of the edges of the gap from the depressions noted in the density of states plots. The results with the amorphous RDF agree better with the experimental results than those obtained with the liquid RDF.

[1] F. Herman and J. P. Van Dyke, Phys. Rev. Lett. **21**, 1575 [1968].
[2] D. Adler, Critical Reviews in Solid State Sciences **2**, 317 [1971].
[3] F. Herman, N. W. Dalton, and T. R. Koehler, Computational Solid State Physics, Plenum Publishing Co., New York 1972.
[4] N. F. Mott and E. A. Davis, Electronic Processes in Non-Crystalline Materials, Clarendon Press, Oxford 1971.
[5] T. C. McGill and J. Klima, J. Phys. C. Solid State Phys. **3**, L 163 [1970]; Phys. Rev. B **5**, 1517 [1972].
[6] M. H. Cohen, H. Frizsche, and S. R. Ovshinsky, Phys. Rev. Lett. **22**, 1065 [1969].
[7] Y. F. Tsay, D. K. Paul, and S. S. Mitra, Phys. Rev. B **8**, 2827 [1973].
[8] W. A. Harrison, Pseudopotentials in the Theory of Metals, W. A. Benjamin Co., New York 1966.
[9] D. Brust, Phys. Rev. **134**, A 1337 [1964].
[10] V. Heine and D. Weaire, Sol. State Phys. **24**, 249 [1970].
[11] M. L. Cohen and T. K. Bergestresser, Phys. Rev. **141**, 789 [1969]; T. K. Bergestresser and M. L. Cohen, Phys. Rev. **164**, 1069 [1967].

[12] J. D. Joannopoulos and M. L. Cohen, Phys. Rev. B **7**, 2644 [1973]; ibid. **8**, 2733 [1973].
[13] D. Weaire, Phys. Rev. Lett. **26**, 1541 [1971].
[14] D. Weaire and M. F. Thorpe, Phys. Rev. B **4**, 2508 [1971]; M. F. Thorpe and D. Weaire, Phys. Rev. Lett. **27**, 1581 [1971].
[15] B. Kramer, Phys. Stat. Sol. (b) **41**, 649 [1970]; ibid. **47**, 501 [1971].
[16] H. Richter and G. Breitling, Z. Naturforsch. **13a**, 988 [1958].
[17] S. C. Moss and J. F. Graczyk, Proc. Tenth Intl. Conf. Phys. Semiconductors, USAEC, 658 (1970).
[18] W. E. Spicer and T. M. Donovan, Phys. Lett. **36** A, 85 [1971]; W. E. Spicer, T. M. Donovan, and J. E. Fisher, J. Non-Crystalline Solids **8—10**, 122 [1972].
[19] D. T. Pierce and W. E. Spicer, Phys. Rev. B **5**, 3017 [1972].
[20] L. D. Laude, R. F. Willis, and B. Fitton, Solid State Comm. **12**, 1007 [1973].
[21] L. Ley, S. Kowalczyk, R. Pollak, and D. A. Shirley, Phys. Rev. Lett. **29**, 1088 [1972].
[22] P. Jena and N. C. Halder, Phys. Rev. B **6**, 2131 [1972].
[23] N. C. Halder, the Properties of Liquid Metals, edited by S. T. Takeuchi, Taylor and Francis Ltd., London 1973.
[24] A. O. E. Animalu and V. Heine, Phil. Mag. **12**, 1249 [1965].
[25] N. C. Halder and C. N. J. Wagner, J. Chem. Phys. **45**, 482 [1966]; N. C. Halder and P. Jena, J. Chem. Phys. **57**, 1830 [1972].
[26] N. W. Ashcroft and J. Lekner, Phys. Rev. **145**, 83 [1966]; J. E. Enderby and D. M. North, J. Phys. Chem. Liquids **1**, 1 [1968].
[27] D. Henderson and F. Herman, J. Non-Crystalline Solids **8—10**, 359 [1972].
[28] R. Kaplow, S. L. Strong, and B. L. Averbach, Phys. Rev. **138**, 1336 [1965].
[29] D. Henderson and I. Ortenburger, Computational Solid State Physics, Plenum Publishing Co., New York 1972.
[30] C. Kittel, Introduction to Solid State Physics, Fourth Edition, Wiley and Sons, Inc., New York 1971.